International Journal of Applied Engineering Research
ISSN 0973-4562 Volume 2, Number 4 (2007), pp. 595–607

http://www.ripublication.com/ijaer.htm

Compact Finite Difference Investigation of Pressure Field Governed by a Three Dimensional Wave Equation

M. J. Maghrebi, M. Farzaneh and M. Shariati

Faculty of Mech. Eng., Shahrood Uni. of Tech., Shahrood, I. R. Iran
E-mail : javad@shahroodut.ac.ir

Abstract

Numerical Simulation of three dimensional wave equation is conducted in a cubic domain which contains two parts, part A and part B. Part A of the domain is a $\cap$-shaped empty channel, containing air, and part B, containing a solid medium, is the difference between the whole cubic domain and part A. A Dirichlet type boundary condition is specified at the inlet boundary. At all other boundaries of the cubic domain a null Neumann boundary conditions are imposed. As an initial condition a null pressure distribution is specified everywhere in the cubic domain except at the inlet boundary. All spatial derivatives are calculated using a compact finite difference scheme. Computations are advanced in time using a compact third order Runge-Kutta scheme. These computations have to be performed twice in succession for each sub-time step of the Runge-Kutta scheme. The numerical code is successfully tested against an exact solution. This issue is followed by the discussion of a three-dimensional simulation. These results, for pressure, are then integrated over the entire surface of the end plane to introduce the load applied to the plane. Both results indicates that the compact finite difference simulation of the wave equation produce a satisfactory and reliable result.

Keywords: Compact Finite Difference; Pressure Field; Three Dimensional Wave Equation; Reflecting Boundary Conditions.

Introduction

The extension of the piecewise exponential method (PEM) for the case of multidimensional wave problems was studied by Zalizniak [1]. This was performed on the basis of operator splitting and the PEM scheme for the one-dimensional wave

equation. He provided numerical results for two problems of wave propagation in comparison with the analytical solutions.

A direct numerical model was developed for determining the transverse wave forces that act on an asymmetric structure on a submerged permeable breakwater in a three-dimensional, non-breaking wave field by Dong-Soo et.al. [2]. The model combined the volume of fluid (VOF) method and the porous body model to accurately simulate the nonlinear interaction between water waves and a porous structure. He performed laboratory experiments which revealed the validity of the numerical model. The propagation of waves in two-dimensional and three-dimensional bounded visco-elastic medium was described in the space frequency domain, leading to a Helmholtz-type boundary value problem, which is non coercive, non-Hermitian, and complex valued by Taeyoung et.al.3].

They derived first-order absorbing boundary conditions and used to minimize spurious reflections from the artificial boundaries. They described the global procedures for the approximate solution of the problem. For the spatial discretization they use rectangular nonconforming finite element methods. Mattsson and Jan Nordstrom [4] derived high order finite difference approximations in rectangular geometries for the second order wave equation with discontinuous coefficients. The proposed method was verified by 1-D and 2-D numerical simulations. Sreekanth et.al. [5] developed a spectral finite element with embedded transverse crack to simulate the diagnostic wave scattering in composite beams with various forms of transverse crack.

The results of numerical simulations for comparing with 2D finite element prediction showed the efficiency of the method to predict the crack location and overall trends due to various crack configurations. An efficient numerical algorithm for solving viscous and non-viscous wave equations were developed by Hyeona et.al[6]. A three-level second-order implicit algorithm were used without introducing auxiliary variables.

A locally one-dimensional procedure which has a splitting error not larger than the truncation error was suggested to solve problems of diagonal diffusion tensors in cubic domains. Both the three-level algorithm and its locally one dimensional procedure were proved to be unconditionally stable. An error analysis for the numerical solution of viscous waves were performed to show the accuracy and the efficiency of the new algorithms for the propagation of acoustic waves. Finite volume evolution Galerkin schemes for the three-dimensional wave equation system were derived by Lukacova et.al.[7]. Numerical experiments proved the accuracy and the multidimensional behavior of the solutions.

In this paper the numerical simulation of three dimensional wave equation is performed using the compact finite difference scheme for the spatial derivatives and the compact third order Runge-Kutta scheme for temporal derivative. The pressure is taken as the field variable and the governing equation is solved for pressure. Initial condition, which are the pressure distribution and the time rate of the pressure are set to zero everywhere within the domain. Boundary conditions are reflected type boundary condition on every plane of the boundary except at the inlet. The inlet of computational domain is forced by a function which varies with time. The numerical

experiment is validated against an exact solution of the wave equation. The proposed method reveals the potential and applicability of the numerical analysis for solving the hyperbolic type governing equations.

Governing Equation

The wave equation is governed by a hyperbolic differential equation. That is

$$\frac{\partial^2 p}{\partial t^2} = c^2 \nabla^2 p \tag{1}$$

where

- C is the wave speed regarded as the material's property of the medium.
- $\nabla^2 = \frac{\partial^2}{\partial x^2} + \frac{\partial^2}{\partial y^2} + \frac{\partial^2}{\partial z^2}$
- p, pressure, is the field variable.

The wave equation is solved in a cubic domain.

The computational domain with the coordinate system used are shown in Fig.(1). The domain consists of two parts with different properties. Part A of the domain is a $\cap$ shaped, containing air, and part B, which is the difference between the whole cubic domain and part A, contains soil. The whole of the computational domain, which is cubic, is divided into equal increments in the x,y and z directions. The grid sizes in each spatial directions are denoted by Δx , Δy and Δz respectively.

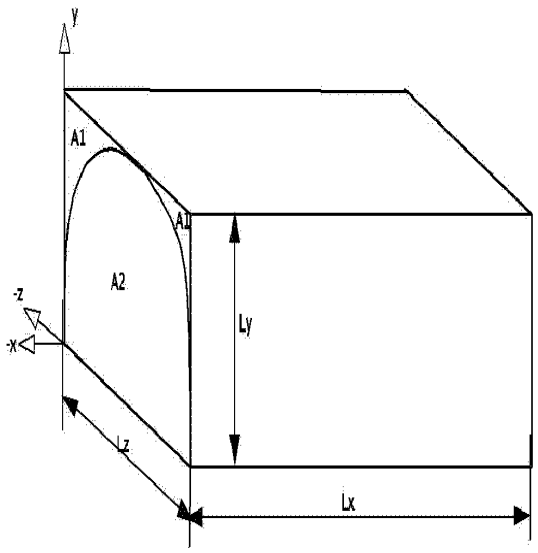

Figure 1: Computational domain.

Boundary and Initial Conditions

Since both temporal and spatial derivatives appeared in the governing equation are second order, two initial conditions and two boundary conditions, in each spatial

direction, are needed. The initial conditions are pertaining to pressure p and the time derivative of pressure $\frac{\partial p}{\partial t}$ at $t=0$. Both of these distributions are set to zero within the domain except at the inlet boundary which is specified according to the inlet forcing condition. Dirichlet type boundary condition is specified at the inlet boundary of the computational domain. At all other boundaries a null Neumann boundary condition is used. This is due to the fact that the rate of change of pressure in a solid medium is negligible in compare with the rate of change of pressure in a gas medium such as air. Since the end plane is solid the outflow boundary condition is also facilitated by a null Neumann type boundary condition.

Modeling of Spatial Derivatives

The right hand side of the governing equation contains Laplacian operator. The second derivatives in the Laplacian in each spatial direction is evaluated using the compact finite difference scheme of Lele [8]. According to the scheme the second derivative in any spatial direction, say (x), is modeled implicitly as Eq.(2).

$$p''_{j-1} + \frac{1}{\alpha} p''_j + p''_{j+1} = \frac{4(\frac{1}{\alpha} - 1)}{3\Delta x^2}(p_{j-1} - 2p_j + p_{j+1}) + \frac{(10 - \frac{1}{\alpha})}{12\Delta x^2}(p_{j-2} - 2p_j + p_{j+2}) \quad (2)$$

where $\alpha = \frac{1}{4}$

At the immediate vicinity of the boundaries (at $j=1$ and $j=J-1$), the second-order compact finite difference scheme Eq.(2) is used with $\alpha = \frac{1}{10}$. At $j=0$, a one-sided, third order scheme is used. That is:

$$p''_0 + 11p''_1 = \frac{1}{\Delta x^2}(13p_0 - 27p_1 + 15p_2 - p_3) \quad (3)$$

At the solid boundary of ($j=J$) the following form which meets the null derivative boundary condition [9] is employed.

$$p''_J + 2p''_{J-1} = \frac{-3}{2\Delta x^2}(p_J - p_{J-2}) \quad (4)$$

In other two spatial directions (y,z) an analogous approach used for determining the second derivatives in (x) are used. The exceptions relate to $y=0$ and $z=0$ planes where the null derivative must be imposed. At these boundaries the following form is used. For example at $y=0$ plane:

$$p''_0 + 2p''_1 = \frac{-3}{2\Delta y^2}(p_0 - p_2) \quad (5)$$

The accuracy of the numerical scheme representing the second spatial derivative is illustrated in Fig.(2). The figure shows the order of accuracy for

$p(x) = \sum_{k=-N/2}^{N/2} \hat{p}(k) \exp(2\pi ikx / Lx) + c.c.$ when the preceding compact finite difference scheme is used for determining the second derivative. Here *c.c.* denotes a complex conjugate.

In constructing the right hand side of the wave equation the wave speed must be considered as appropriate for each part. In other words, the wave speed for the grids in part A and B of the computational domain must be set as the air and soil wave speeds, respectively. The field variable, *p*, is updated for whole of the domain at the same time and this is not computed for each part *A* and *B* individually. Owing to this fact and as the governing equation for both parts are the same no explicit boundary conditions are required at the common surfaces between the *A* and *B* parts. When solving for the both parts, the boundary conditions pertains to the external surfaces of the cubic domain and the interaction between the common surfaces are implicitly treated by the wave equation. This strategy is very similar to determining the support reactions of a truss in which the internal joint reactions are not appeared in the free body diagram of the whole truss body.

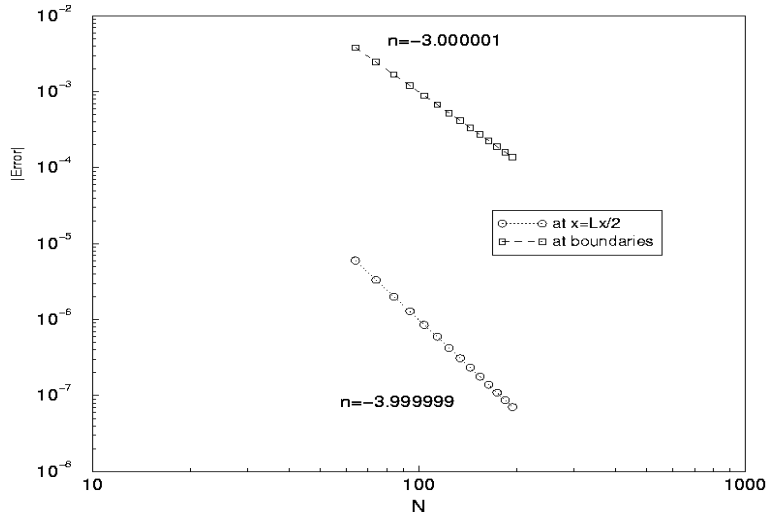

Figure 2: Order of accuracy for second derivative approximation using compact finite difference scheme

Table 1: Third order Runge-Kutta time advancement scheme

First location	Second location
u^n	$R(u^n)$
$u^{'} = u^n + c_1 \Delta t R$	$R^{'} = R(u^{'})$
$u^{''} = u^{'} + (c_2 R^{'} + d_2 R)\Delta t$	$R^{''} = R(u^{''})$
$u^{n+1} = u^{''} + (c_3 R^{''} + d_3 R^{'})\Delta t$	

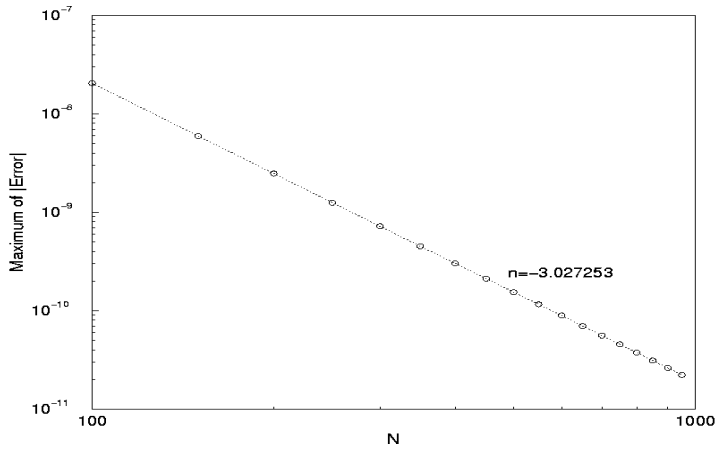

Figure 3: Order of time advancement scheme for $\frac{du}{dt} = -u(t)$ with $u(0) = 1.$

Time Advancement Scheme

Wray A. [8] developed a compact, third order, Runge-Kutta scheme. This is used here to advance the computations in time. According to this scheme, the time advancement of the following model equation

$$\frac{du}{dt} = R(u) \tag{6}$$

is performed in three sub-steps as described in Table.(1).The table shows that the time advancement of Eq.(6) by one time increment Δt requires computation of the right-hand side (R) in three successive sub-time-steps. In each of these sub-steps, time (t) is incremented by $(c_i + d_i)\Delta t$ and u is accumulated by linear combination of R's associated with the current time level and that of the previous sub-time-step. Results in the second column of the third sub-time-step is regarded as the solution incremented by Δt. The coefficient used in the time advancement scheme (c_i, d_i) can be obtained using the Taylor series expansion for R' and R'' and equating the terms of like orders. This leads to

$$c_1 + c_2 + c_3 + d_1 + d_2 + d_3 = 1$$

$$c_1 c_2 + c_3[\frac{d_2}{c_2}(1 + \frac{d_3}{c_3}) + c_2(1 + \frac{d_2}{c_2})] = \frac{1}{2}$$

$$c_1{}^2 c_2 + c_3[c_1 + c_2(1 + \frac{d_2}{c_2})]^2 + c_1{}^2 d_3 = \frac{1}{3}$$

$$c_1 c_2 c_3 = \frac{1}{6}$$

There are two parameter families of solutions to the preceding set of

equations. The scheme will be self-starting if $d_1 = 0$.
One parameter families of solution to the set of equations is,

$$c_1 = \frac{2}{3}, d_1 = 0$$
$$c_2 = \frac{5}{12}, d_2 = \frac{-5}{12}$$
$$c_3 = \frac{3}{5}, d_3 = \frac{-4}{15}$$

Detailed discussion can be studied in Maghrebi [8]. A test case is performed to validate the order of accuracy for the Rung-Kutta time advancement scheme applied to the following equation.

$$\frac{du}{dt} = -u(t)$$

This equation has an exact solution of $u(t) = e^{-t}$ if $u(0) = 1$ is taken as the initial condition. The Eq. (7) is solved for $u(t)$ at $t = 1$ using different time increments. The results, indicating the maximum errors between the numerical results and the exact solution, are illustrated in Fig.(3). This definitely ensures the third order of accuracy for the time advancement of the computation.

Since the wave equation is a second order differential equation with respect to time, time advancement of the simulation is performed in two successive steps. Since $\frac{\partial^2 p}{\partial t^2} = \frac{\partial}{\partial t}(\frac{\partial p}{\partial t})$ the wave equation can be written as $\frac{\partial g}{\partial t} = c^2 \nabla^2 p$ where $\frac{\partial p}{\partial t} = g(x, y, z, t)$. In other words, the first step in the time advancement of the governing equation is to form the right hand side of $\frac{\partial g}{\partial t} = c^2 \nabla^2 p$ using initial condition for p. The second step is to update the initial condition for $g(x, y, z, t)$ using $\frac{\partial p}{\partial t}$ as the initial condition. Note that both initial conditions are used to update g.

Next, $\frac{\partial p}{\partial t} = g(x, y, z, t))$ is updated for p. The right-hand side of the equation $g(x, y, z, t)$ is not evaluated as preceding part but it is explicitly specified as the second initial condition. Here also both initial conditions are used to update p. Note that the updated distributions for g and p are regarded as new initial conditions which will be used for the next sub-steps in the time advancement process. These computations, according to the compact third order Runge-Kutta scheme, are repeated over three sub-steps to advance the solution by one time increment. Application of the

preceding process must be implemented N time steps to obtain the solution at the end of the time interval.

Code Verification

The numerical code is validated against an exact solution of a three dimensional case. The solution to the three dimensional wave equation will converge to $p(x, y, z, t) = \sin(x)\cos(y)\cos(z)\sin(\sqrt{3}t$ if $p(x, y, z, t = 0) = 0$ and $\frac{\partial p}{\partial t}(x, y, z, 0) = \sqrt{3}\sin(x)\cos(y)\cos(z)$ are used as the initial conditions. The inlet boundary conditions must also be specified as $p(0, y, z, t) = 0$. Parameters used in this test case are chosen such that the null Neumann boundary conditions exist at all of the solid boundaries. Hence, $L_x = \frac{\pi}{2}$, $L_y = \pi$, $L_z = 2\pi$. The spatial resolution of the simulation is $10 \times 40 \times 40$, $c^2 = 1$ for both parts of the domain. The results for the L^2 norm of the error within the entire of the computational domain after advancing the simulation one thousand time steps is found to be $2.409996e^{-12}$ which definitely ensures the accuracy of the numerical simulation conducted.

Input File Structure

The code is written such that the input data file can be easily generated. The construction of an input data file for the next three dimensional simulation is as follows.

```
Length of the domain in x------= 15.
Length of the domain in y------= 5.
Length of the domain in z------= 4.
C_Air----------------= 340.
C_Soil---------------= 2000.
time increment-----------= .00001
number of the grids in x------= 60
number of the grids in y------= 20
number of the grids in z------= 16
number of substeps---------= 3
number of time steps--------= 4421
Amplitude of oscillation-Pf-----= 100000.
Bi----------------= 1.
Step Numbers Required 4 impact time-= 10
```

The multiplication of the last entry of the data file by the time increment is the time period shown by T in Eq.(8).

Three Dimensional Simulation

The results of the pressure time history at $x = L_x$, $y = L_y / 2$, $z = L_z / 2$ in one, two and three dimensional simulations are shown in Fig.(5). It is observed that the maximum pressure occurs at $t = \frac{L_x}{c}$. The next maximum is observed at $t = \frac{3L_x}{c}$. Both of these values correspond to the time required for the wave to reflect form the exit, $x = L_x$, and the inlet, $x = 0$, boundaries.

The results of pressure time history in a much smaller time extents of $0.04 \le t \le 0.05$ are shown in Fig.(6) to clearly illustrate the time variation of the pressure around the maximum. The figure indicates that the maximum pressure corresponding to the one dimensional simulation is much higher than that of the two and three dimensional simulations. This is because of the damping property of the null Neumann type boundary conditions. In one, two and three dimensional simulations one, three and five boundaries are facilitated by the damping conditions, null Neumann boundary conditions, respectively. The three dimensional simulation of the wave equation has been terminated at a time corresponding to the maximum pressure. At this time level the pressure distribution is plotted as in Fig.(4).

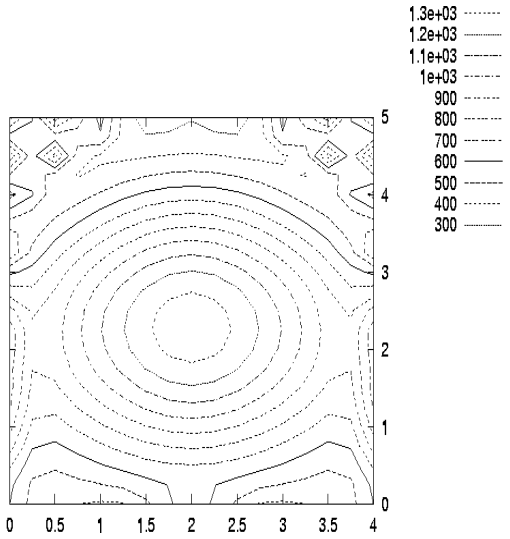

Figure 4: Pressure iso-levels on the outlet boundary of the domain.

Since $z = L_z / 2$ is the line of symmetry, it is expected to obtain a symmetric pressure distribution about $z = L_z / 2$. This is clearly observed in Fig.(4). Careful examination of the figure also reveals that the maximum of the pressure locates at the centroid of the $\bigcap$ shaped empty channel (section A).

The time corresponding to the maximum load is shown to be approximately $t = \frac{L_x}{c}$. The other maximums relate to the time with odd coefficients of $t = \frac{L_x}{c}$ (i.e. $t = \frac{3L_x}{c}$, $t = \frac{5L_x}{c}$,…) approximately. These results are coincided with the response of the wave due to reflection from the streamwise boundaries in x.

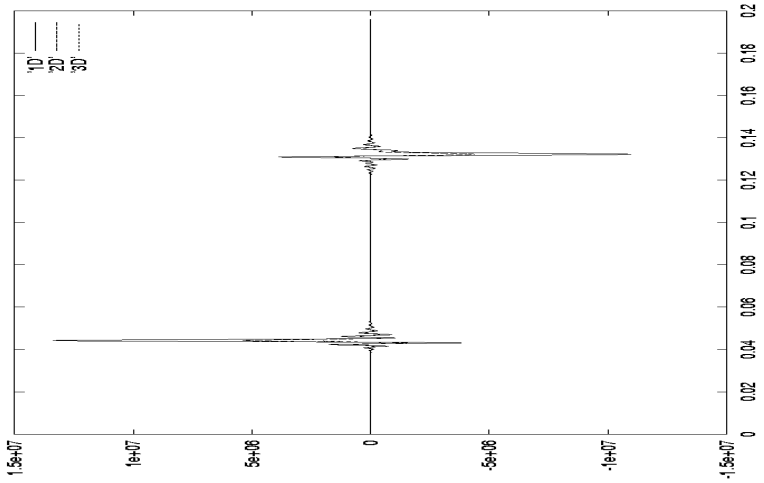

Figure 5: Pressure time history.

Since the storage of pressure field at any instance in the computational domain is very memory demanding and time consuming, the integral of pressure on the end plane is calculated. This is indeed the surface integral of pressure over the entire of the end plane ($x = L_x$). In other words, the time history of the resulting force $F(L_x, t)$ applied to the end plane of the computational box is calculated and recorded.

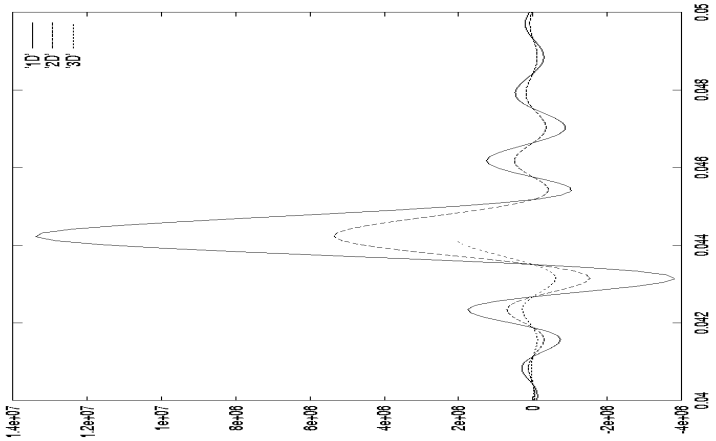

Figure 6: Pressure time history in one, two and three dimensional simulation

$$F(x,t) = \int_A p(x, y, x, t)dA$$

where A is the cross-sectional area representing the end plane of the computational domain. Shown in Fig.(7) is the force applied on A due to the pressure distribution.

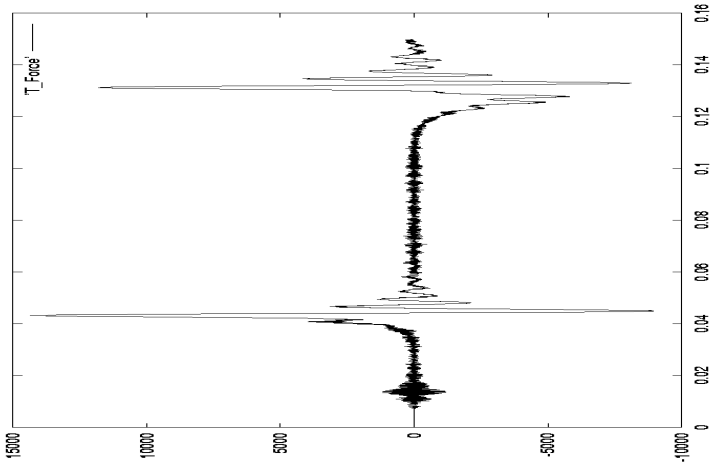

Figure 7: Time history of load applied to section *A* of the end plane.

The magnitude of the force has to be less than $L_y L_z P_f = 4 \times 6 \times 10^5$. This fact is clearly observed in Fig.(7) for three-dimensional simulation. According to the numerical investigations performed on the code, it was observed that the location of maximum load is altered when the size of the computational box is changed. It was also investigated that the time corresponding to the maximum load is $t = \frac{L_x}{c}$ exactly, if the wave speed in different mediums are assumed to be the same.

To find the maximum pressure distribution on the end plane of the computational domain, two entries in the data file are adjusted carefully. These two entries are time increment and the number of time steps. The multiplication of these two entries is the critical time at which the load is found to be maximum. Since the code is thoroughly verified, any divergence or discrepancy will be related to the stability requirement. In other words, the time increment must be small enough to ensure the restriction and the requirement of CFL number. Otherwise, the simulation will be diverged quickly. The CFL condition has not been studied analytically, using Von Neumann stability analysis say, but the value must not exceed 0.7 according to the numerical investigation performed on the code.

The inlet boundary condition of the simulations were introduced according to

$$p(x = 0, y, z, t) = P_f (1 - \frac{t}{T}) e^{\frac{-bt}{T}} \tag{8}$$

where $P_f = 100000$ and $b = 1$.

This boundary condition is imposed at the entire of the inlet boundary regardless of the solid or the air medium.

.

Conclusions

The numerical simulation of the three dimensional wave equation was conducted in a cubic domain containing two parts, part *A* and part *B*. Part *A* of the domain was a $\cap$ shaped, containing air, and part *B*, containing soil, was the difference between the whole domain and part *A*. A Dirichlet type boundary condition was specified at the inlet boundary. Other conditions imposed at the solid boundaries were the null normal derivatives. Null pressure distribution was supplied for the initial conditions everywhere in the domain except at the inlet boundary. Spatial derivatives in any directions were calculated using a compact finite difference scheme. For each time increment computations were advanced in time using compact third order Runge-Kutta scheme which has to be applied twice in succession in each sub-time step. The numerical code was successfully validated against an exact solution. The load time trace which was the surface integral of the pressure applied to the end plane of the computational domain were generated and discussed. The numerical results revealed that the modeling of the three dimensional wave equation using the compact finite difference and the compact third order Runge-Kutta schemes produced a reliable and satisfactory results.

References

[1] Zalizniak, V., The piecewise exponential method (PEM) for the numerical simulation of wave propagation: a multidimensional wave problem, Computer Methods in Applied Mechanics and Engineering, Volume 178, Issues 1-2, July 1998, Pages 115-124

[2] Dong-Soo Hur, Norimi Mizutani and Do-Sam Kim, Direct 3-D numerical simulation of wave forces on asymmetric structures Coastal Engineering, Volume 51, Issues 5-6, August 2004, Pages 407-420

[3] Taeyoung Ha, Juan E. Santos and Dongwoo Sheen, Nonconforming finite element methods for the simulation of waves in viscoelastic solids, Computer Methods in Applied Mechanics and Engineering, Volume 191, Issues 49-50, 6 December 2002, Pages 5647-5670

[4] Ken Mattsson and Jan Nordstrom, High order finite difference methods for wave propagation in discontinuous media, Journal of Computational Physics, Volume 220, Issue 1, 20 Dec. 2006,Pages 249-269.

[5] D. Sreekanth Kumar, D. Roy Mahapatra and S. Gopalakrishnan, A spectral finite element for wave propagation and structural diagnostic analysis of composite beam with transverse crack, Finite Elements in Analysis and Design, Volume 40, Issues 13-14, August 2004, Pages 1729-1751.

[6] Hyeona Lim, Seongjai Kim and Jr, Jim Douglas, Numerical methods for viscous and nonviscous wave equations, Applied Numerical Mathematics, Volume 57, Issue 2, February 2007, Pages 194-212.

[7] M. Lukacova-Medvid'ova, G. Warnecke and Y. Zahaykah, Finite volume evolution Galerkin (FVEG) methods for three-dimensional wave equation system, Applied Numerical Mathematics, November 2006, In Press.

[8] M.J. Maghrebi., A Study of the Evolution of Intense Focal Structures in Spatially Developing Three-Dimensional Plane Wakes, PhD Thesis, Monash University, 1999.

[9] S.K. Lele., Compact Finite Difference Schemes with Spectral-Like Resolution, J. Comp. Phys., Vol 103, pp 16-42, 1992.